Journal of Power Sources 185 (2008) 302–310

Contents lists available at ScienceDirect

Journal of Power Sources

journal homepage: www.elsevier.com/locate/jpowsour

The effect of air stoichiometry change on the dynamic behavior of a proton exchange membrane fuel cell

Shuguo Qu, Xiaojin Li*, Ming Hou, Zhigang Shao, Baolian Yi

Fuel Cell R&D Center, Dalian Institute of Chemical Physics, Chinese Academy of Sciences, Dalian 116023, China

ARTICLE INFO

Article history:
Received 9 May 2008
Received in revised form 28 June 2008
Accepted 30 June 2008
Available online 9 July 2008

Keywords:
Polymer electrolyte fuel cells
Transient response
Stoichiometric change
Voltage undershoot
Reactant starvation

ABSTRACT

Numerical simulations are carried out in this paper, to study the effect of air stoichiometry change on a single-channel proton exchange membrane (PEM) fuel cell undergoing load change. For this purpose, the air stoichiometry change rate and pattern, as well as its lagging time to the load change and initial value, are taken into account in this model, respectively. The transient response of cell potential to load change has been investigated and the undershoot behavior has been observed. Detailed results are further presented to show the transient response of the cell in terms of local current density and oxygen mass fraction distributions. This work shows that the extent of air dilution/starvation down the channel depends on the air stoichiomtric flow ratio change rate, pattern, etc. It is also shown this undershoot can be eliminated by adjusting the initial air flow ratio, or by improving the air flow ratio change rate, etc. Finally, the validity of the numerical model in this paper is verified by the comparison between the model results and experimental data, showing that this numerical model can be resorted to reveal the effects of air stoichiometry change on the dynamic behavior of a PEMFC.

1. Introduction

PEM fuel cell is regarded as a potential future power source for electrical vehicles, due to its high efficiency, zero emission and fast start-up at room temperature. As power source for transportation, electrical vehicle often operate dynamically, which easily cause some harmful phenomena occurring in fuel cell [1–3]. For example, during start-up and acceleration of electrical vehicles, the reactant starvation will occur in fuel cell. In the case of fuel starvation on anode, carbon corrosion and water electrolysis will occur [2], according to:

Carbon corrosion:

$$C + 2H_2O \rightarrow CO_2 + 4H^+ + 4e^-$$

Water electrolysis:

$$2H_2O \rightarrow O_2 + 4H^+ + 4e^-$$

In the case of oxidant starvation on cathode, hydrogen pump will occur [2], according to:

Hydrogen pump:

$$2H^+ + 2e^- \rightarrow H_2$$

The presence of hydrogen on cathode could chemically generate heat on the platinum particles and result in the local hot spots in the MEA, which could lead to failure of the fuel cells [3]. The acceleration degradation will shorten the fuel cell life. So the main aim of transient behavior research is to eliminate these harmful phenomena in fuel cell and to prolong the fuel cell life.

Over the last two decades, there has been growing interest in studying the transient behavior of PEMFC. Generally, the published works in this field can be classified into experimental studies [4–9], semi-empirical modeling [10–12] and mechanistic modeling. The mechanistic modeling can be further divided into single-phase [13–22] and two-phase [23–26] approaches. For experimental research, Van Zee group [4–6] indicated the possibility of overshoot behavior dependent on the rate of voltage change, and stoichiometry. Shen et al. [9] studied the effect of pre-supplied air stoichiometry on cell voltage by applying a variable air stoichiometry during load change. For the semi-empirical modeling, it combines theoretically derived differential and algebraic equations with empirically determined relationships. Zhang et al. [10] proposed a semi-empirical model based on the measurements from a Nexa™ PEM fuel cell module under different load conditions. Semi-

* Corresponding author. Tel.: +86 411 84379051; fax: +86 411 84379185.
E-mail address: xjli@dicp.ac.cn (X. Li).

0378-7753/$ – see front matter © 2008 Elsevier B.V. All rights reserved.
doi:10.1016/j.jpowsour.2008.06.080

Nomenclature

a	specific area of electrode (cm^{-1})
A_{ch}	cross-sectional area of flow channel (cm^2)
A_{MEA}	area of the MEA (cm^2)
C_{H_2}	local hydrogen concentration ($mol\,m^{-3}$)
$C^{ref}_{H_2}$	reference hydrogen concentration ($mol\,m^{-3}$)
C_{O_2}	local oxygen concentration ($mol\,m^{-3}$)
$C^{ref}_{O_2}$	reference oxygen concentration ($mol\,m^{-3}$)
D	diffusion coefficients ($m^2\,s^{-1}$)
E_{cell}	cell operating potential (V)
E_{oc}	open-circuit voltage (V)
F	Faraday's constant = 96,487 ($C\,mol^{-1}$)
i_a	anode local current density ($A\,cm^{-2}$)
i_c	cathode local current density ($A\,cm^{-2}$)
$i^{ref}_{0,a}$	anode reference exchange current density ($A\,cm^{-2}$)
$i^{ref}_{0,c}$	cathode reference exchange current density ($A\,cm^{-2}$)
I	cell operating current density ($A\,cm^{-2}$)
k_p	hydraulic permeability (m^2)
M_{H_2}	molecular weight of hydrogen ($kg\,mol^{-1}$)
M_{H_2O}	molecular weight of water ($kg\,mol^{-1}$)
M_{O_2}	molecular weight of oxygen ($kg\,mol^{-1}$)
n_d	electro-osmotic drag coefficient
p	pressure (atm)
R	universal gas constant ($8.314\,J\,mol^{-1}\,K^{-1}$)
T	temperature (K)
$\mathbf{u}$	velocity vector ($m\,s^{-1}$)
W	species mass fraction (dimensionless)

Greek letters

ε	porosity
η	overpotential
μ	viscosity ($kg\,m^{-1}\,s^{-1}$)
ρ	density ($kg\,m^{-3}$)
σ	electrode electronic conductivity ($S\,m^{-1}$)
ξ	stoichometric flow ratio

empirical modeling is very useful for making quick predictions on the dynamics of fuel cell stacks or systems. However, it cannot provide an adequate physical understanding of the phenomena inside the cell [27]. For numerical research, mechanistic modeling has received much attention for better understanding of the main transient processes in PEM fuel cells, including species transport, membrane hydration/dehydration, heat transfer, etc. Among these, the species transport in the flow channel and the gas diffusion layer (GDL) is of importance on fuel cell dynamics. References [17,18,22] have studied the species transport process and its effect on the dynamics of the cell. For example, Shimpalee et al. [17] studied the effect of rate change of cell voltage on the magnitude of current overshoot and found the peak of current overshoot depends on the rate of change of the voltage and the amount of gas flow rate. Um et al. [18] proposed a 2D transient model and studied the effects of hydrogen dilution along the anode gas channel. It is noted that all the predictions except Ref. [22] take a step change of stoichiometric flow ratio (stoic) or constant cathode/anode flows during load change to study the transient behavior of fuel cell. Hu and Fan [22] take into account the effect of variable flow rate on the dynamic behavior of fuel cell by adopting a sinusoidal change of air stoichiometry while keeping other parameters constant. However, to our knowledge, no numerical study has been reported by applying a variable flow rate during load change.

The objective of this work is to study the effects of air stoichiometry changes on the transient behavior of the fuel cell by applying an increase in air stoichiometry during loading, and the emphasis is placed on the four different aspects of air stoichiometry change, including its rate and pattern, as well as its lagging time to the load change and initial value. By applying the 2D, isothermal, time-dependent model proposed in this work, the effects of these four different aspects on the transient characteristics of cell potential and mass transport are investigated, respectively.

2. Model development

2.1. Model assumptions

The assumptions and simplifications adopted in the present model are:

(1) The cell operates under isothermal conditions at 80 °C.
(2) The gas mixture is an incompressible ideal fluid.
(3) The flow in the gas channel is laminar.
(4) The diffusion layer, catalyst layer and membrane are isotropic and homogeneous, and the membrane is impermeable to gas species.
(5) Ohmic potential drops in the diffusion layers and bipolar plates are neglected due to their high electrical conductivities.
(6) The contact resistance between any two parts in the fuel cell is neglected.
(7) The catalyst layer is considered as a thin interface between membrane and diffusion layer.
(8) Reactant gases dissolving in the electrolyte at the catalyst are not taken into account.

2.2. Computational domain

Fig. 1 shows the schematic diagram of a PEM fuel cell with a single channel for this model.

2.3. Governing equations

In this paper, the transient, two-dimensional, multi-component, isothermal and single phase transportation model can be written in a single domain forms as follows:

Continuity:

$$\frac{\partial \rho}{\partial t} + \nabla \cdot (\rho \vec{u}) = S_m \tag{1}$$

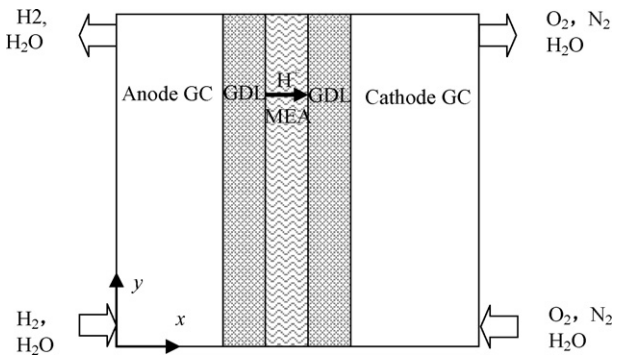

Fig. 1. The schematic diagram of PEM fuel cell with a single channel.

Table 1
Source terms for governing equations in various regions of a PEMFC

	GDL	CL, a	CL, c	Membrane
Mass	$S_m = 0$	$S_m = M_{H_2}S_{H_2} + M_{H_2O}S_W^a$	$S_m = M_{H_2O}S_{O_2} + M_{H_2O}S_w^c$	$S_m = 0$
Momentum	$S_u = -\frac{\mu}{K_p}\vec{u}$	$S_u = -\frac{\mu}{K_p}\vec{u}$	$S_u = -\frac{\mu}{K_p}\vec{u}$	/
	$S_{H_2} = 0$	$S_{H_2} = -\frac{i_a}{2F}$	$S_{H_2} = 0$	$S_{H_2} = 0$
Species	$S_{O_2} = 0$	$S_{O_2} = 0$	$S_{O_2} = -\frac{i_c}{4F}$	$S_{O_2} = 0$
	$S_w = 0$	$S_w^a = -\frac{n_d}{F}i_a$	$S_w^c = \frac{n_d}{F}i_c + \frac{i_c}{2F}$	$S_w = 0$

Momentum:

$$\frac{1}{\varepsilon}\left[\frac{\partial\rho\vec{u}}{\partial t} + \frac{1}{\varepsilon}\nabla\cdot(\rho\vec{u}\vec{u})\right] = -\nabla p + \nabla\cdot\tau + S_u \quad (2)$$

Species:

$$\frac{\partial c_k}{\partial t} + \nabla\cdot(\vec{u}c_k) = \nabla\cdot(D_k^{eff}\nabla c_k) + S_k \quad (3)$$

Source terms in the above governing equations are summarized in Table 1 for various sub-domains of the fuel cell. In the gas channels, the porosity ε becomes unity, and Eq. (2) becomes the conventional form of the momentum equation. In the porous media region, the source term in momentum conservation equation, S_u, represent Darcy's drag force.

The source terms in Eqs. (1)–(3) are directly related to the electrical current, through which the transport equations are coupled with electrochemical processes. In this work, the electrical current is modeled by the Butler–Volumer equation [16,28,29] as follows:

Anode:

$$i_a = ai_{0,a}^{ref}\left(\frac{C_{H_2}}{C_{H_2,ref}}\right)^{1/2}\left[\exp\left(\frac{\alpha_a^a}{RT}F\eta_a\right) - \exp\left(\frac{\alpha_c^a}{RT}F\eta_a\right)\right] \quad (4)$$

Cathode:

$$i_c = ai_{0,c}^{ref}\left(\frac{C_{O_2}}{C_{O_2,ref}}\right)\left[\exp\left(\frac{\alpha_a^c}{RT}F\eta_c\right) - \exp\left(\frac{\alpha_c^c}{RT}F\eta_c\right)\right] \quad (5)$$

where a_a^a, a_a^c, a_c^c and a_a^c are the anodic and cathodic charge transfer coefficient.

2.4. Physical and transport properties

The water content and the flux of water in the membrane are important for membrane conductivity, which have a great influence on cell performance and local current density distribution. In this model, the water transport equation in the entire MEA region is encompassed in the general form of Eq. (3), where the source/sink terms are detailed in Table 1. The first term of S_W^a and S_W^c in Table 1 represents the electro-osmotic drag, and the second source term of S_W^c is the water generation from ORR in the cathode catalyst layer. For the first source term, n_d is introduced to stand for the electro-osmotic drag coefficient, which has been correlated by Springer et al. [30] to the membrane water content, λ, and water activity, a. The physical parameters of membrane, such as EW, ρ_{dry} and ε_m, are shown in Table 2.

In the mass transport equation, the diffusion coefficient of species k, D_k, varies in different sub-regions of the PEM fuel cell, depending on the physical phase of species k. In the anode and cathode gas channel, the diffusion coefficient is calculated as a function of temperature and pressure [31]. For the porous regions of a PEM fuel cell such as the gas diffusion and catalyst layers, the expression is modified into the effective species, D_k^{eff}, using Bruggman correlation [32].

$$D_k = D_0\left(\frac{T}{T_0}\right)^{3/2}\left(\frac{P}{P_0}\right) \quad \text{for gas channel}$$

$$D_k^{eff} = \varepsilon_i^{1.5}D_k \quad \text{for porous regions}$$

where D_0 is the diffusivity in gas channel at standard condition. The mass diffusivities of hydrogen and oxygen through the membrane are usually a few orders lower than that in gas and are taken to be constant. Table 2 lists the geometries, physical parameters and operating conditions used in this model.

Table 2
Geometries, physical parameters and operating conditions

Parameter	Symbol	Value
Channel length	L_{ch}	20 mm
Channel width	W_{ch}	1 mm
Gas diffusion layer thickness	t_{gdl}	260 μm
Membrane thickness (Nafion 112)	t_m	51 μm
Porosity of anode/cathode gas diffusion layers	ε_{gdl}	0.6
Volume fraction of ionomer in catalyst layer	ε_m	0.26
H_2 reference mole concentration,	$C_{H_2}^{ref}$	40.88 mol m^{-3}
O_2 reference mole concentration,	$C_{O_2}^{ref}$	40.88 mol m^{-3}
Anode exchange current density multiply specific area	$ai_{0,a}^{ref}$	5.0×10^7 A m^{-3}
Cathode exchange current density multiply specific area	$ai_{0,c}^{ref}$	1.2×10^2 A m^{-3}
Anode charge transfer coefficient for anode reaction	a_a^a	0.5
Cathode charge transfer coefficient for anode reaction	a_c^a	0.5
Anode charge transfer coefficient for cathode reaction	a_a^c	0.5
Cathode charge transfer coefficient for cathode reaction	a_c^c	0.5
Permeability of membrane	K_m	1.8E−18 m^2
Permeability of anode/cathode gas diffusion layers	K_{gdl}	2.0E−12 m^2
Dry membrane density	ρ_{dry}	2000 kg m^{-3}
Equivalent weight of electrolyte in membrane	EW	1.1 kg mol^{-1}
Faraday constant	F	96487 C mol^{-1}
Universal constant	R	8.314 J mol^{-1} K^{-1}
H_2 diffusivity in membrane	$D_{H_2}^m$	2.59×10^{-10} m^2 s^{-1}
O_2 diffusivity in membrane	$D_{O_2}^m$	1.22×10^{-10} m^2 s^{-1}
H_2 diffusivity in the anode gas channel at standard condition	$D_{0,H_2,c}$	1.1×10^{-4} m^2 s^{-1}
H_2O diffusivity in the anode gas channel at standard condition,	$D_{0,W,a}$	1.1×10^{-4} m^2 s^{-1}
O_2 diffusivity in the cathode gas channel at standard condition	$D_{0,O_2,c}$	3.2×10^{-5} m^2 s^{-1}
H_2O diffusivity in the cathode gas channel at standard condition	$D_{0,W,c}$	7.3×10^{-5} m^2 s^{-1}
Cell temperature	T	353 K
Humidity of anode inlet stream (%)	RH	100
Humidity of cathode inlet stream (%)	RH	100
Pressure at the inlet of anode gas channel	$P_{in,a}$	1 atm
Pressure at the inlet of cathode gas channel	$P_{in,c}$	1 atm
Anode stoichiometric flow ratio	ξ_a	2.0

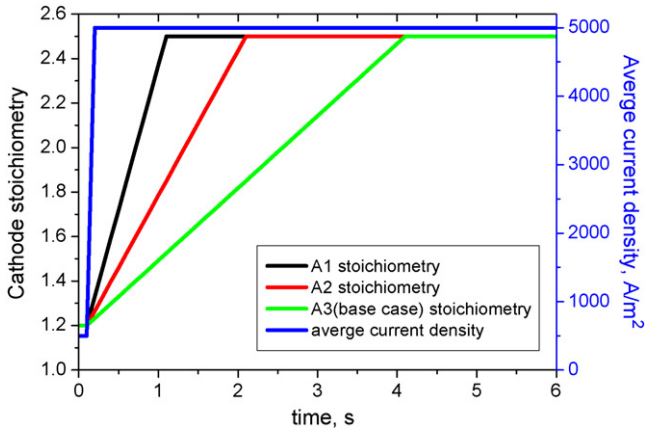

Fig. 2. Cell average current density and cathode stoichiometry changes with time for case A.

2.5. Cell potential and current density

Taking account the polarization losses, the actual cell voltage of a fuel cell, E_{cell}, can be calculated as

$$E_{cell} = E_{oc} - \eta_{act} - \eta_{ohm,\ mem} - \eta_{conc} \quad (6)$$

where E_{oc} is the open-circuit voltage, η_{act} the activation polarization, $\eta_{ohm,mem}$ the ohmic polarization and η_{conc} the concentration polarization. It is noted that the ohmic loss offered by contact resistance is neglected. The activation losses can be calculated from the Butler–Volmer equation. The open-circuit voltage [33], the ohmic and concentration losses [34] can be represented as follows:

$$E_{oc} = 0.2329 + 0.0025T \quad (7)$$

$$\eta_{ohm,mem} = IR_{mem} \quad (8)$$

$$\eta_{conc} = \frac{RT}{nF} \ln\left(1 - \frac{I}{I_L}\right) \quad (9)$$

where T is the cell temperature, I_L is the limiting current density, R_{men} the resistance caused by the electrolyte membrane to the flow of H^+ ions, which depends on the thickness of the membrane, t_m, and the proton conductivity of the membrane, σ_m, and is represented by the expression:

$$R_{mem} = \frac{t_m}{\sigma_m} \quad (10)$$

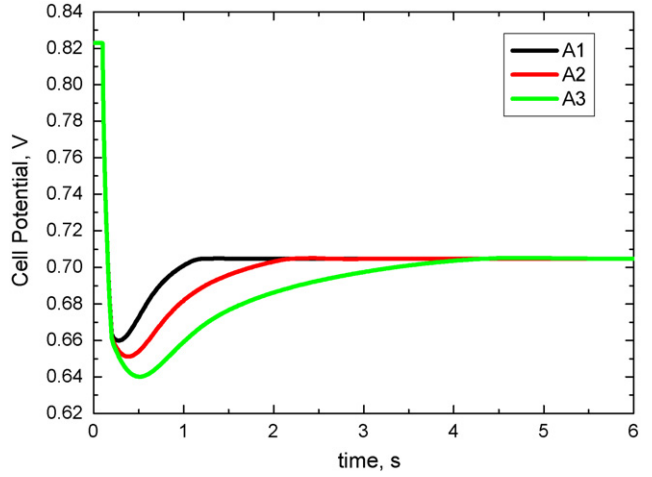

Fig. 3. Transient response of cell voltage changes with time for case A.

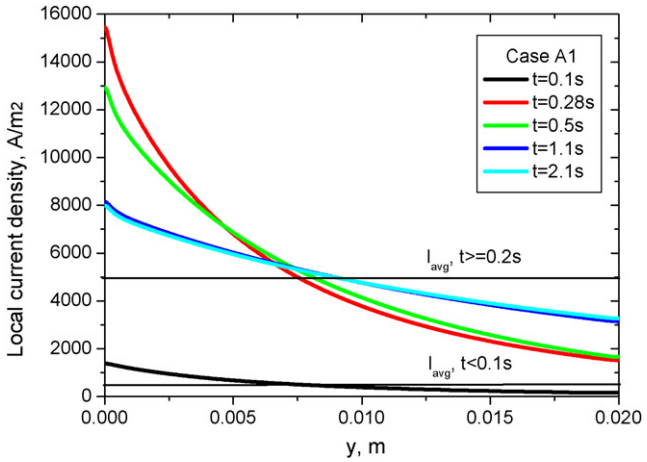

Fig. 4. Local current density distributions on the cathode catalyst layer along channel direction for case A1.

σ_m has been modeled by Springer et al. [30] in 1991. In the past decade, several related models have been proposed subsequently [35–37]. However, those models are quite complicated and the physical parameters in the models are difficult to be determined. In comparison, the membrane conductivity given by Springer et al. is expressed in water content and temperature in a simple formula and these two parameters in the formula can be easily determined. So this model is wildly accepted and used in most of the numerical studies on PEM fuel cell.

2.6. Boundary and initial conditions

2.6.1. Inlet boundaries

The inlet values at the anode and cathode are prescribed for the velocity and species concentrations (Dirichlet boundary conditions). At the gas channel inlet, the inlet velocity u_{in}, is expressed by the respective reactant stoichiometric flow ratio of anode and cathode, ξ_a and ξ_c, defined based on the desired operating current density, I, as follows:

$$u_{in,a} = \xi_a \frac{I}{2F} \frac{RT}{p_{in,a}} \frac{A_m}{A_{ch,a}} \frac{1}{X_{H,in}} \quad (11)$$

$$u_{in,c} = \xi_c \frac{I}{4F} \frac{RT}{p_{in,c}} \frac{A_m}{A_{ch,c}} \frac{1}{X_{O,in}} \quad (12)$$

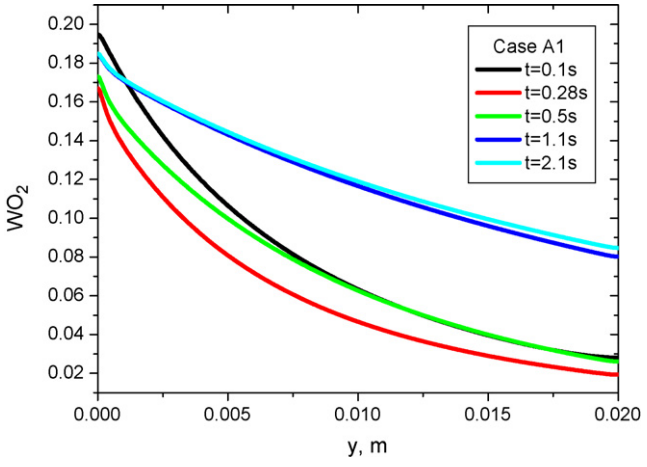

Fig. 5. Local oxygen mass fraction distributions on the cathode catalyst layer along channel direction for case A1.

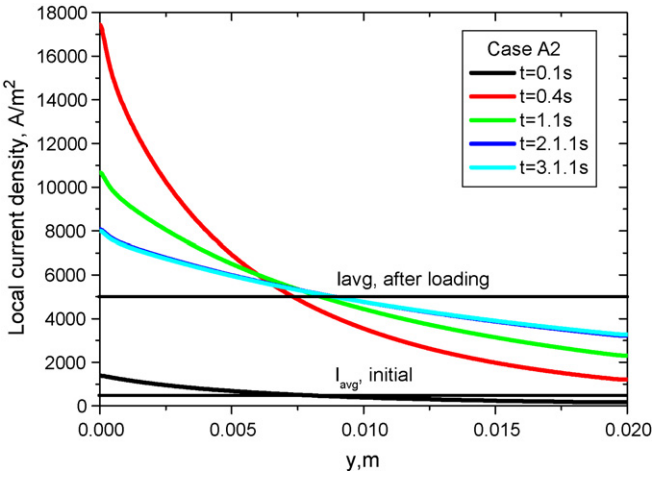

Fig. 6. Local current density distributions on the cathode catalyst layer along channel direction for case A2.

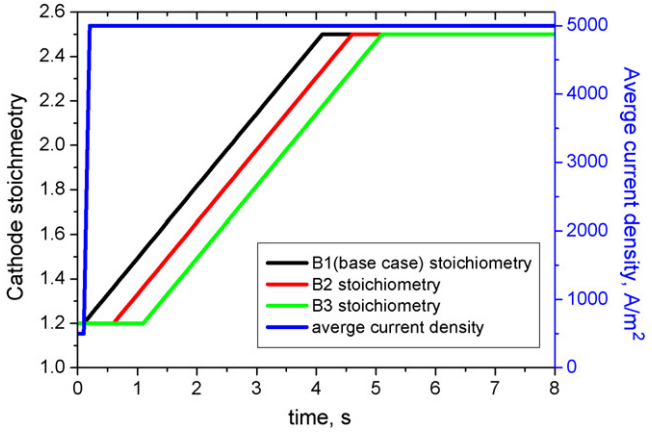

Fig. 8. Cell average current density and cathode stoichiometry changes with time for case B.

where A_m is the geometrical area of the membrane and A_{ch} is the cross-sectional area of the gas channel. X_H is molar fraction of hydrogen and X_O molar fraction of oxygen at the gas channel inlet.

2.6.2. Outlet boundaries

At the outlet of the gas-flow channels, only the pressure is being prescribed as the desired electrode pressure. For all other variables, fully developed or no-flux conditions are applied on the gas channel outlet (Neumann boundary conditions):

$$\frac{\partial \vec{u}}{\partial n} = 0, \frac{\partial c_k}{\partial n} = 0 \quad (13)$$

2.6.3. Wall

No-slip and impermeable velocity condition and no-flux condition are adopted

$$\vec{u} = 0, \frac{\partial c_k}{\partial n} = 0, \frac{\partial p}{\partial n} = 0 \quad (14)$$

2.7. Numerical procedure

The time-dependent conservation equations are discretized by the finite element method and solved by FemLab software. Stringent numerical tests are conducted to achieve the mesh size and time step independence for the numerical solution. It is shown that the computation conducted on a mesh size of 5453 elements with first time interval $\Delta t = 0.001$ s is satisfactory and these choices are used in this work to understand the transient behavior of the reactant gas transport in PEM fuel cells and its effect on cell performance. Due to the memory and time requirements for the iteration process, the FemLab software is run on Dell Precision workstation (Intel Xeon 2.2 GHz, 1.5 GB SDRAM).

3. Result and discussion

In this section, the effects of the cathode stoichiometry change on the transient characteristics of a single cell with straight channel to load change are studied. In this study, the cell average current density is used to view the load change and a linear increment from 50 to 500 mA cm^{-2} in 0.1 s is applied on all the simulation cases. Note that the value of air stoichiometry in the whole text is given corresponding to 500 mA cm^{-2}, not to the temporary current density. For the cathode stoichiometry, its change rate and pattern, its lagging time to the load change and initial value, are investigated and considered as an input to study its effect on the cell performance, respectively.

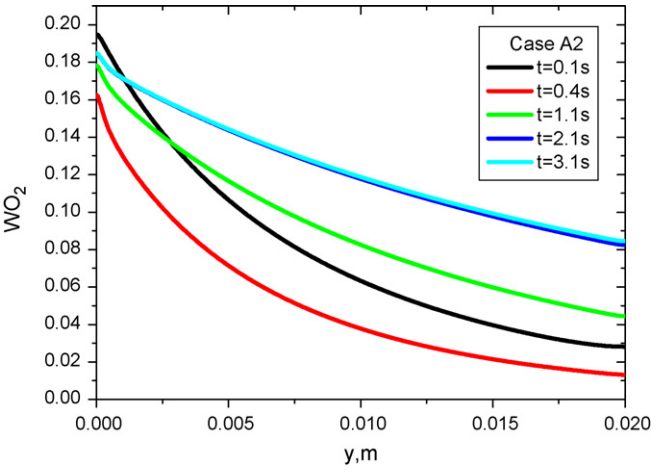

Fig. 7. Local oxygen mass fraction distributions on the cathode catalyst layer along channel direction for case A2.

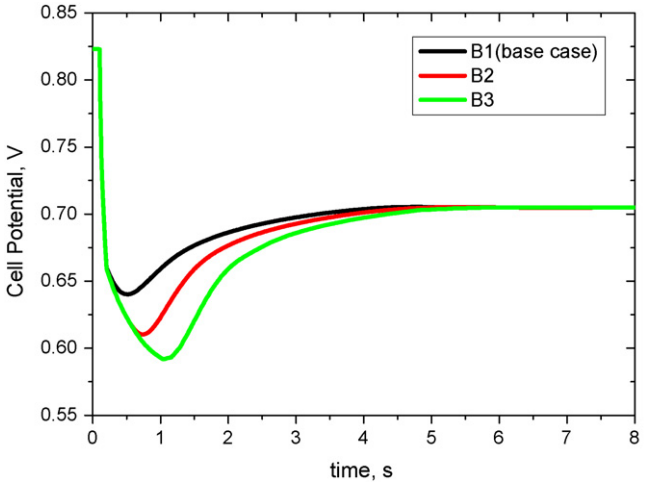

Fig. 9. Transient response of cell voltage changes with time for case B.

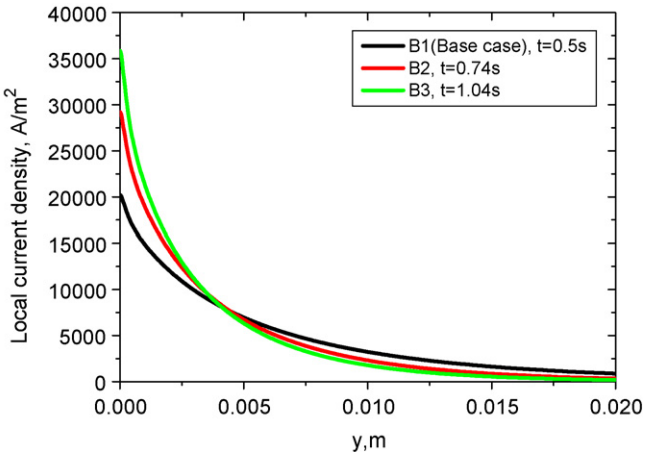

Fig. 10. Local current density *d* distributions on the cathode catalyst layer along channel direction for case B.

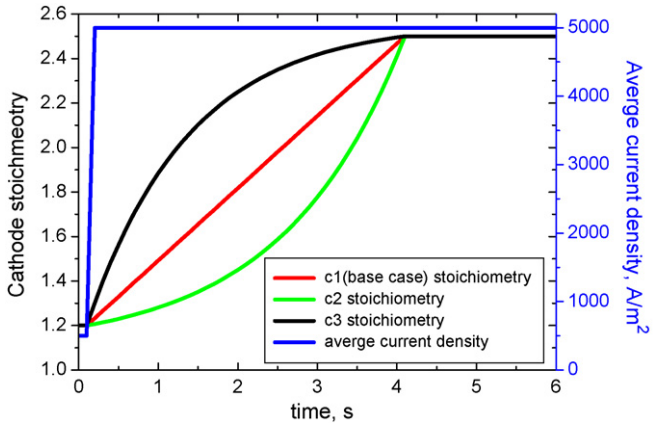

Fig. 12. Cell average current density and cathode stoichiometry changes with time for case C.

3.1. Effects of air stoichiometry change rate

Most of predictions take a step change of stoichiometric flow ratio (stoic) or constant cathode/anode flows during load change to study the transient behavior of fuel cell. For example, Shimpalee et al. takes a constant cathode/anode flows to study the effects of cell voltage change rate on cell performance, which corresponds to an initial stoic of 2.6/4.4 (2.6 for anode and 4.4 for cathode flow) at 0.7 V and a final stoic of 1.2/2.4 at 0.5 V. However, in practice, i.e., fuel cell engine for electrical vehicle, during the vehicle start-up or acceleration, the hydrogen/air flow rates increase corresponding to the cell output. So, to make the simulations approaching the practical circumstance, it is necessary to study the effect of the cathode stoichiometry change rate on the transient behavior of PEMFCs. In this study, three different air stoic rates, from 1.2 to 2.5 in 1 s (case A1), in 2 s (case A2), in 4 s (case A3), are inputted to view its effects on cell transient behavior. The operating current density and the air stoic changes with the time are shown in Fig. 2.

Fig. 3 gives the transient response of cell potential at three different air stoic rates. For the three potential curves, they have the common starting point of 0.82 V and the same steady value of 0.70 V, corresponding to the same initial and final conditions for the three cases. In this fig., it is clearly seen that the magnitude of cell potential overshoot is affected by the slope of air stoic growth. Lower gas stoic change rate results in greater cell voltage undershoot, lower peak of cell voltage and a longer time to reach the steady state. For case A1, the cell voltage decreases initially and reaches the minimum value of 0.66 V at $t = 0.28$ s. And then it increases with time and reaches the steady value at $t = 1.2$ s. When the air stoic change rate is slower as for case A2, the cell voltage has a minimum value of 0.65 V at $t = 0.4$ s and reaches the steady value at $t = 2.2$ s. And the minimum cell voltage is 0.64 V at $t = 0.5$ s and the time of reaching the steady state is $t = 4.2$ s for case A3.

Figs. 4 and 5 give the local current density and the local air mass fraction profiles on the cathode catalyst layer along the channel direction at different times for case A1. In Fig. 4, the lower curve gives the initial local current density distribution with an average value of 50 mA cm^{-2}. And the upper four curves give the local current density distribution after loading, with an average of 500 mA cm^{-2}. Compared the upper four curves, lower and more non-uniform current density is clearly seen downstream along the channel direction during the load change, particularly under the arising of voltage undershoot peak. This can be easily explained by Eq. (5), due to the rapid depletion of oxygen from the inlet to outlet, shown in Fig. 5. When $t \geq 1.1$ s, the cell approaches its final state, with more uniform and higher current density and oxygen mass fraction along the channel direction.

Similar to the analysis of case A1, the simulation cases A2 and A3 are also analyzed. Figs. 6 and 7 give the local current density and

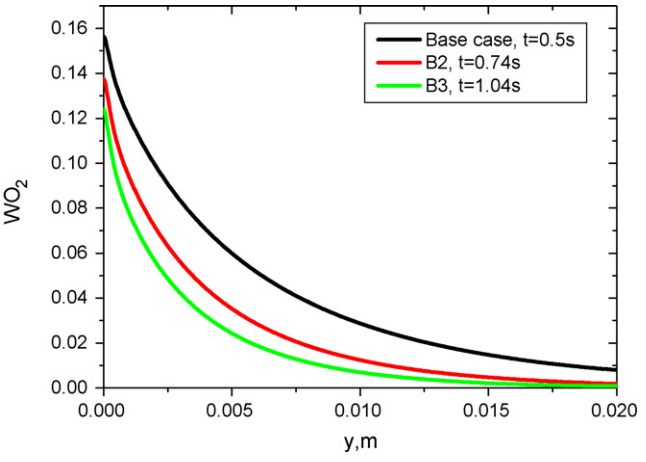

Fig. 11. Local oxygen mass fraction distributions on the cathode catalyst layer along channel direction for case B.

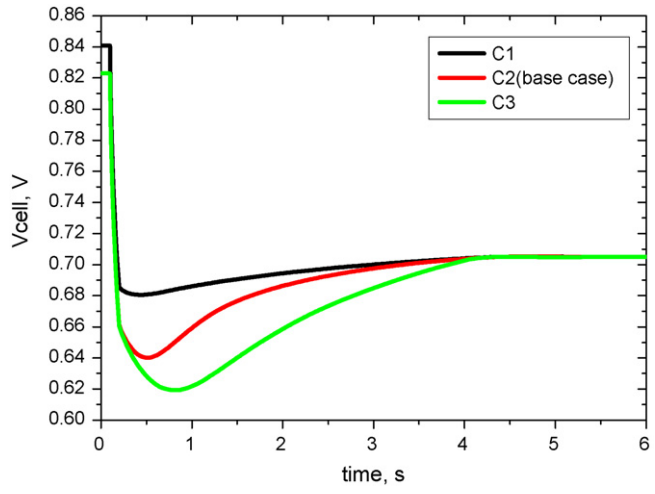

Fig. 13. Transient response of cell voltage changes with time for case C.

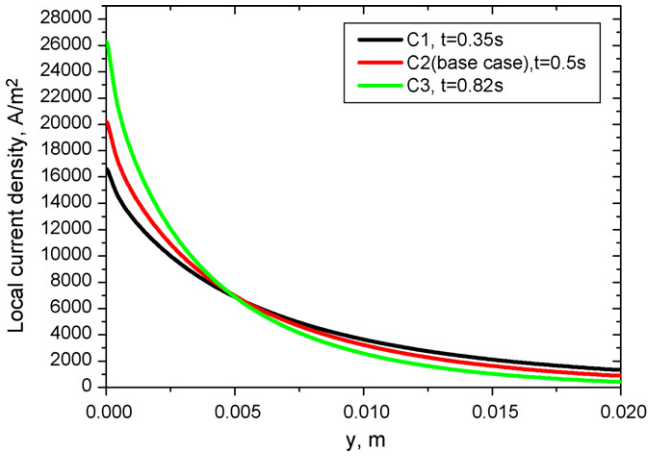

Fig. 14. Local current density distributions on the cathode catalyst layer along channel direction for case C.

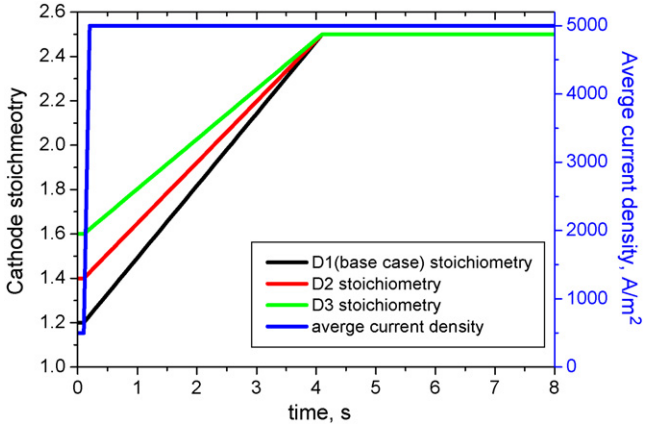

Fig. 16. Cell average current density and air stoichiometry changes with time for case D.

the local air mass fraction distributions on the cathode catalyst layer along the channel at different times for case A2. Compared to case A1, case A2 shows more non-uniform current density distribution down the channel during load change (Fig. 6). This trend is more apparent when the voltage undershoot peak arises ($t = 0.4$ s), due to a lower increasing rate of air stoichiometry of case A2, resulting in a much heavier reactant dilution/starvation down the channel (Fig. 7), and thus a substantially larger polarization loss according to Eq. (5). For case A3, its air stoichiometry increasing rate is the lowest of the three cases, resulting in the heaviest reactant dilution/starvation down the channel during load change, and thus the largest activation over-potential for oxygen reduction reaction (ORR) is required to sustain a specific operating current density.

3.2. Effects of lagging time to load change

In this section, the effects of lagging time of air stoichiometry response to load change on the transient behavior is investigated. For fuel cell usage, i.e., fuel cell engine for electrical vehicle, during start-up or acceleration, the air compressor need a response time to the load change. This time is called the lagging time of the air flow to load change. In this paper, case A3 without lagging time is used as base case (case B1), and two lagging times, 0.5 s (case B2) and 1 s (case B3), are considered as input to investigate its effects on the cell performance (seen in Fig. 8).

Fig. 9 gives the transient response of cell potential to the load change at different level of lagging time. It shows that the peak of voltage undershoot depends on the level of lagging time. Longer lagging time results in greater cell voltage undershoot, lower peak of cell voltage and a longer time to reach the final state. For case B2, the cell voltage decreases initially and reaches the minimum value of 0.60 V at $t = 0.74$ s. And then it increases with time and reaches the steady value at $t = 4.7$ s. Due to a longer lagging time of air stoic to load change for case B3, the cell voltage curve shows a lower minimum value of 0.58 V at $t = 1.24$ s and reaches the steady value at $t = 5.2$ s.

Next, the local current density distribution, as well as the air mass fraction distribution on the catalyst layer along the channel are investigated, as shown in Figs. 10 and 11. For convenience, only the distributions at the peak of cell voltage are considered. Comparison of the three cases, case B3 has the lowest current density downstream along the flow channel, due to the much lower oxygen mass fraction along the channel direction. This is because case B3 has a longer lagging time of air stoic response to load change than cases B1 and B2, resulting in a much heavier reactant dilution/starvation down the channel.

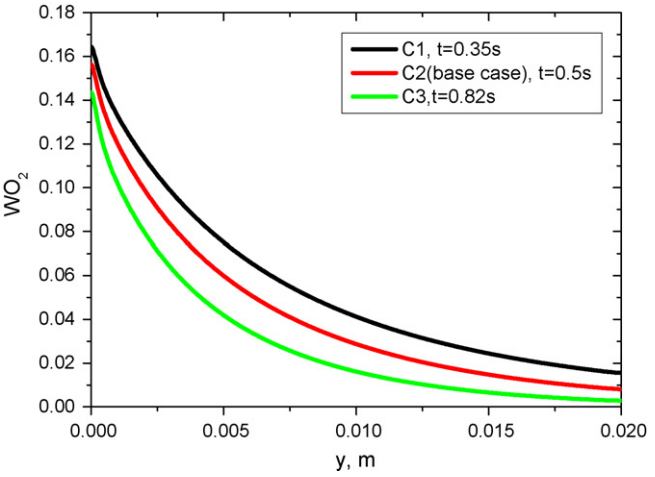

Fig. 15. Local oxygen mass fraction distributions on the cathode catalyst layer along channel direction for case C.

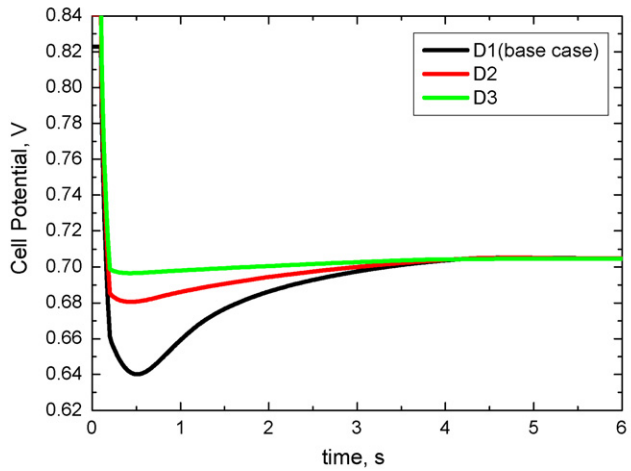

Fig. 17. Transient response of cell voltage changes with time for case D.

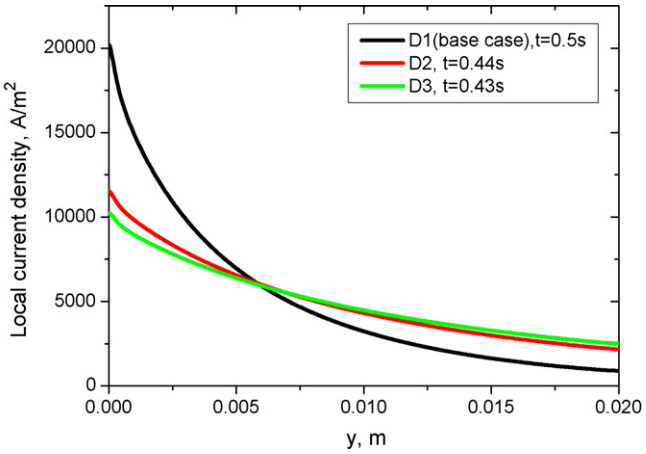

Fig. 18. Local current density distributions on the cathode catalyst layer along channel direction for case D.

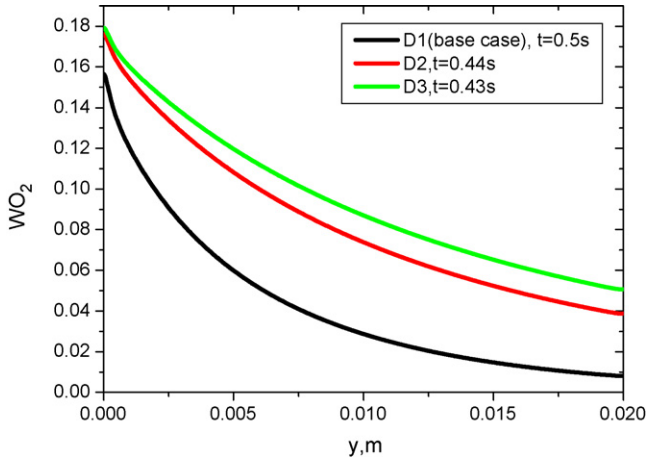

Fig. 19. Local oxygen mass fraction distributions on the cathode catalyst layer along channel direction for case D.

3.3. *Effects of air stoic change pattern on PEMFC characteristics*

In this section, the effect of air flow increasing pattern on the transient behavior of PEM fuel cell is investigated. For example, for the fuel cell engine for transportation, during the start-up and acceleration of the vehicle, the air flow flux shows a parabolic growth, corresponding to the output characteristic of air compressor. However, no numerical or experimental work on the effects of air stoic increasing form, to our knowledge, has been reported. So in this paper, a parabolic increasing of air stoic (case C1) is considered as input to investigate its effect on the transient behavior of fuel cell. For comparison, an exponential increasing (case C3) is also used in this paper. Fig. 12 gives the profiles of parabolic, exponential and linear increasing (base case) of air stoic over time.

Fig. 13 gives the cell voltage variations with time at different shapes of air stoic growth. It is seen that the undershoot phenomena is almost eliminated for case C1. For further analysis, the local current density and air mass fraction distribution occurring at the peak of cell voltage are also investigated, as shown in Figs. 14 and 15. In Fig. 14, a more higher and uniform distribution of local current density is clearly seen downstream along the channel for case C1, due to a more higher oxygen mass fraction down the channel on the catalyst layer, shown in Fig. 15. This is because the air stoic grows much faster for case C1 than cases C2 and C3, largely eliminating reactant dilution/starvation during the load change. Whereas, for case C3, the oxygen is almost depleted downstream along the channel and a larger cathode polarization loss occurs.

3.4. *Effects of initial air stoichiometry*

In this section, the effect of initial air stoichiometry on cell performance is investigated. For this purpose, three different initial air flow ratios, 1.2 (base case), 1.4 (case D2) and 1.6 (case D3) is applied in the simulations as input to investigate its effect on the transient behavior of fuel cell. Though the initial conditions are different, they reach the same final value in 4 s for all three cases. The time profiles of average current density, and air stoichiometry are shown in Fig. 16.

Fig. 17 gives the transient variation of cell potential at different initial air flow ratio. For the case D3 with an initial stoic of 1.6, it has a peak of cell potential of 0.68 V, approaching to the steady value of the cell. This shows that the initial air stoic has a great influence on the cell dynamic behavior, and that the cell voltage undershoot could be eliminated when a proper initial stoic is implemented. The local current density, as well as the air mass fraction along the channel is investigated, as shown in Figs. 18 and 19. Due to the higher initial value of air flow ratio, case D2 and case D3 have a much higher reactant concentration on the catalyst layer downstream along the channel direction, largely eliminating the reactant dilution/starvation down the channel. It is seen that the down-the-channel effect can be alleviated by applying an adequate air stoichiometric flow ratio.

4. Model validation

In this section, our numerical simulation was compared with available experimental data in the literature to validate the model proposed in this paper. As have been discussed in the introduction, many researchers have studied the dynamic behavior of PEM fuel cell experimentally [4–9]. However, most of studies in the literature are concentrated on either step change of stoichiometric flow ratio or constant cathode/anode flow rate during load change to study the transient behavior of fuel cell [4–8]. As far as we know, only Shen et al. [9] from our group take into account a variable flow rate during load change. So the experimental data of Ref. [9] is used to verify the validity of the proposed model in this paper.

The validation process consists of simulating the model by applying the experimental inputs as model inputs, and then comparing experimental outputs with the simulated results. In Ref. [9],

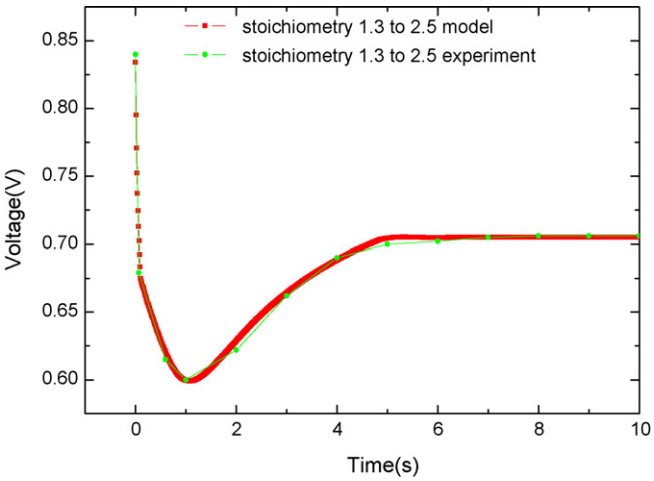

Fig. 20. Comparison between model and experimental cell voltage evolution from Fig. 7 in [9].

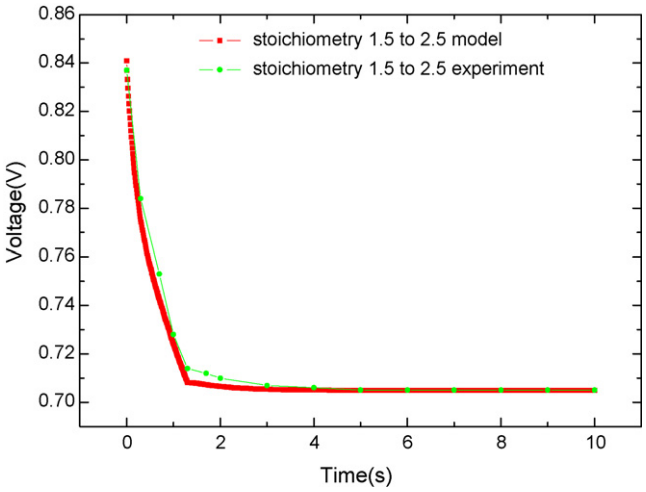

Fig. 21. Comparison between model and experimental cell voltage evolution from Fig. 8 in [9].

the voltage change of PEMFC over time when loading dynamically from 50 to 500 mA cm^{-2} in 0.5 s was provided and the effect of pre-supplied air stoichiometry on the dynamic behavior was investigated. Two cases were simulated, one with air stoic change from 1.3 to 2.5 in 4 s, and the other from 1.5 to 2.5 in 4 s. The simulated cell voltage evolutions at different pre-supplied air stoichiometry are given in Figs. 20 and 21 and compared with the experimental data. It is found that the model predictions match the experimental data quite closely. Thus, the validity of the numerical model presented in this paper is verified.

5. Conclusions

A 2D, isothermal, dynamic model has been presented to study the effect of air stoichiometry change on a single-channel polymer electrolyte fuel cell (PEFC). Four different aspects of air stoic change, including the rate and pattern, as well as the lagging time to load change and the initial value, are taken into account in this model, respectively. The cell potential changes with time are investigated and the undershoot behavior in cell potential is observed. It is shown that the air flow ratio changes have a great influence on the cell dynamic response to load change. Detailed results are further presented to show the transient response of the cell in terms of local current density and oxygen mass fraction distributions. It is shown that the oxygen is progressively depleted downstream along the gas channel during the load change, resulting in reactant gas dilution/starvation on the reaction zone. In the presence of large air dilution, the over-potential for the oxygen reduction within the catalyst layer significantly increases to sustain a specific operating current density, thus leading to the cell voltage undershoot during load change. It is also shown that this undershoot can be reduced or eliminated by improving the air stoic change rate, or by increasing the initial air stoic flow ratio, etc. Finally, the validity of the proposed model in this paper is verified by the comparison of the simulated cell voltage with the experimental data. The present work is of importance in optimizing the control strategy of PEM fuel cell to improve its performance to load change.

Acknowledgements

This work was financially supported by the National High Technology Research and Development Program of China (863 Program No. 2007AA05Z131) and the National Natural Science Foundation of China (No. 20206030).

References

[1] S.D. Knights, K.M. Colbow, J. St-Pierre, D.P. Wilkinson, J. Power Sources 127 (2004) 127–134.
[2] R. Borup, J. Meyers, et al., Chem. Rev. 107 (2007) 3904–3951.
[3] A. Taniguchi, T. Akita, K. Yasuda, Y. Miyazaki, Int. J. Hydrogen energy 33 (2008) 2323–2329.
[4] S. Kim, S. Shimpalee, J.W. Van Zee, J. Power Sources 135 (2004) 110–121.
[5] S. Kim, S. Shimpalee, J.W. Van Zee, J. Power Sources 137 (2004) 43–52.
[6] S. Kim, S. Shimpalee, J.W. Van Zee, J. Electrochem. Soc. 152 (2005) A1265–A1271.
[7] J. Benziger, E. chia, E. Karnas, J. Moxley, C. Teuscher, I.G. Kevrekidis, AIChE J. 50 (2004) 1889–1900.
[8] Q. Yan, H. Toghiani, H. Causey, J. Power Sources 152 (2006) 36–44.
[9] Q. Shen, M. Hou, X. Yan, D. Liang, Z. Zang, L. Hao, Z. Shao, Z. Hou, P. Ming, B. Yi, J. Power Sources 179 (2008) 292–296.
[10] Z. Zhang, X. Huang, J. Jiang, B. Wu, J. Power Sources 137 (2004) 43–52.
[11] P.R. Pathapati, X. Xue, J. Tang, Renewable energy 30 (2005) 1–22.
[12] A.J. del Real, A. Arce, C. Bordons, J. Power Sources 173 (2007) 310–324.
[13] W. Yan, C. Soong, F. Chen, H. Chu, J. Power Sources 143 (2005) 48–56.
[14] S. Shimpalee, W. Lee, J.W. Van Zee, H. Naseri-Neshat, J. Power Sources 146 (2005) 87–98.
[15] A. Kumar, R.G. Reddy, J. Power Sources 155 (2006) 264–271.
[16] Y. Shan, D. choe, S. Choi, J. Power Sources 165 (2007) 196–209.
[17] S. Shimpalee, D. Spuckler, J.W. Van Zee, J. Power Sources 167 (2007) 130–138.
[18] S. Um, C.Y. Wang, K.S. Chen, J. Electrochem. Soc. 147 (2000) 4485–4493.
[19] W. Wang, C.Y. Wang, Electrochim. Acta 50 (2005) 1307–1315.
[20] H. Ju, H. Meng, C.Y. Wang, Int. J. Heat Mass Transfer 48 (2005) 1303–1315.
[21] S. Shimpalee, W. Lee, J.W. Van Zee, H. Naseri-Neshat, J. Power Sources 156 (2005) 355–368.
[22] G. Hu, J. Fan, J. Power Sources 165 (2007) 171–184.
[23] D. Song, Q. Wang, Z. Liu, C. Huang, J. Power Sources 159 (2006) 928–942.
[24] S. Chang, H. Chu, J. Power Sources 161 (2006) 1161–1168.
[25] M. Hua, J. Power Sources 171 (2007) 738–746.
[26] H. Wu, P. Berg, X. Li, J. Power Sources 165 (2007) 232–243.
[27] D.M. Bernadi, M.W. Verbrugge, J. Electrochem. Soc. 139 (1992) 2477–2491.
[28] V. Gurau, H.T. Liu, S. Kakac, AIChE J. 44 (1998) 2410–2422.
[29] Y. Wang, C.Y. Wang, Electrochem. Acta 51 (2006) 3924–3933.
[30] T.E. Springer, T.A. Zawodzinski, S. Gottesfeld, J. Electrochem. Soc. 138 (1991) 2334–2342.
[31] R.B. Bird, W.E. Stewart, E.N. Lightfoot, Transport Phenomena, John Wiley & Sons, New York, 1960.
[32] R.E. Meredith, C.W. Tobias, Conduction in heterogeneous systems, in: C.W. Tobias (Ed.), Advances in Electrochemistry and Electrochemical Engineering, Interscience Publishers, New York, 1962.
[33] A. Parthasarathy, S. Srinivasan, A.J. Appleby, J. Electrochem. Soc. 139 (1992) 2530–2537.
[34] Fuel Cell Handbook, 5th ed., EG&G Services, Parsons, Inc., US Department of Energy Office of Fossil Energy, National Energy Technology Laboratory, West Virginia, 2000, pp. 2.4–2.8.
[35] J. Fimrite, B. Carnes, H. Struchtrup, N. Djilali, J. Electrochem. Soc. 152 (2005) A1815.
[36] P. Choi, N.H. Jalani, P. Datta, J. Electrochem. Soc. 152 (2005) E123.
[37] L. Pisani, M. Valentin, D.H. Hofmann, L.N. Kuleshova, B. D'Aguanno, Solid State Ionics 179 (2008) 465–476.